

Received January 22, 2021, accepted February 4, 2021, date of publication February 9, 2021, date of current version February 18, 2021.

Digital Object Identifier 10.1109/ACCESS.2021.3058148

A Bionic MEMS Electronic Stethoscope With Double-Sided Diaphragm Packaging

SICUN DUAN¹, WEIDONG WANG¹, SAI ZHANG², XI YANG¹,
YU ZHANG¹, AND GUOJUN ZHANG¹

¹Laboratory of Science and Technology on Electronic Test and Measurement, North University of China, Taiyuan 030051, China

²Department of Physics, Jiangsu University, Zhenjiang 212013, China

Corresponding author: Guojun Zhang (zhangguojun1977@nuc.edu.cn)

This work was supported in part by the National Key Research and Development Project under Grant 2019YFC0119800, in part by the Natural Science Foundation of China through the National Major Scientific Instruments Development Project under Grant 61927807, in part by the National Natural Science Foundation of China under Grant 51875535, and in part by the Fund for Shanxi 1331 Project Key Subject Construction and Innovation Special Zone Project.

ABSTRACT In this paper, an electronic stethoscope is designed based on a bionic Micro-Electro-Mechanical System (MEMS) sound-sensitive sensor. Inspired by the strong sound reflection effect of the water-air interface, a double-sided diaphragm MEMS electronic stethoscope (DMES) encapsulated by a novel double-sided diaphragm packaging is proposed. The double-sided diaphragm packaging's superiority is verified by comparing a single diaphragm MEMS electronic stethoscope (SMES) with DMES. The frequency of the clinical heart sound signal is mostly in the range of 20–600 Hz. Finite simulation results show that for the same incident sound source, the sound pressure level inside double-sided diaphragm packaging is 4dB higher than that of single diaphragm packaging in this frequency band. Furthermore, the actual auscultation test results show that the signal-to-noise ratio (SNR) of DMES reaches 41.3dB, which is 2.2dB higher than SMES. Besides, comparing the heart sound signals collected by DMES and a commercial electronic stethoscope (Model 3200, 3M Littmann, USA), the high consistency of the two signals' characteristic parameters in the time domain and frequency domain proves the feasibility of DMES. Finally, DMES has the advantages of low cost, and its SNR is 10.2db higher than that of the 3M electronic stethoscope. All these show that DMES has a broad prospect in the popularization of basic medical treatment.


INDEX TERMS MEMS, packaging, electronic stethoscope, SNR.

I. INTRODUCTION

The number of deaths caused by Cardiovascular diseases (CVDS) is expected to rise with an increase in the average age of the world's population [1]. However, it is widely known that such mortalities can be prevented if there are a diagnosis and proper follow-up and management from an early stage. Heart sounds transmit specific physiological and diagnostic information such as murmurs and aberrations, which can often be detected before the CVDS [2]. Therefore, cardiac auscultation can be used as an excellent auxiliary diagnostic method; once a problem is detected, proper management and follow up can be carried out. In modern auscultation, electronic stethoscopes have been widely used nowadays. Compared with the conventional stethoscope, the electronic

stethoscope has excellent advantages. For example, the heart sound volume transmitted to the human ear is deficient by using the traditional stethoscope. In contrast, the electronic stethoscope solves this problem by converting sound waves into electrical signals and then appropriately amplifying them to achieve the best listening [3]. Moreover, the electronic stethoscope does not need rich clinical experience and good listening, while it is the opposite in traditional auscultation [4], [5].

For the electronic stethoscope, its sensor and packaging determine its performance together, so they are equally important. Besides, since different sensors are based on various physical principles, electronic stethoscopes made by them may have problems [6]–[8]. There is an electronic stethoscope that is manufactured by mounting a microphone behind the diaphragm of the stethoscope. The intervening air path between the microphone's diaphragm and the diaphragm

The associate editor coordinating the review of this manuscript and approving it for publication was Michail Kiziroglou .

of the stethoscope results in excess ambient noise pickup by the microphone, as well as inefficient acoustic energy transfer [7]. An electronic stethoscope using a piezoelectric sensor receives a signal that is different in tone and distorted compared with the signal received by an acoustic stethoscope [4].

However, the acoustic sensors do not have such problems. In the acoustic field, MEMS technology is widely used. An acoustic sensor based on MEMS is small in size, can be mass-produced, and have better temperature stability. Moreover, its structure can be specifically designed according to specific application requirements, such as perceiving high sound pressure or allowing the hybridization of mechanical and electrical circuits on the PCB [9]–[12].

Xue *et al.* [13] proposed a bionic MEMS sound-sensitive sensor that simulates the working principle of fish's neuromast organ to detect underwater acoustic fields. Because this sensor is very sensitive in the low-frequency band, and the frequency of clinical heart sound signals is mainly concentrated in the low-frequency range of 20–600Hz, an improved version of the sensor, shaped like a lollipop, is adopted to design the electronic stethoscope in this research [14]. Then, considering the packaging's impact on the performance of the electronic stethoscope using the lollipop-shaped sensor, we designed a double-sided diaphragm packaging for it. The double-sided diaphragm packaging adds an extra diaphragm. The extra diaphragm creates a water-air interface since it connects encapsulated liquid inside the packaging and air outside. Theoretical analysis and finite element simulation afterward prove the superiority of double-sided diaphragm packaging. By practical tests, the signal-to-noise ratio (SNR) of double-sided diaphragm MEMS electronic stethoscope (DMES) is higher than that of single diaphragm MEMS electronic stethoscope (SMES) and that of the 3M electronic stethoscope. The characteristic parameters of the heart sound signals collected by DMES and the 3M electronic stethoscope are highly consistent in the time domain and frequency domain.

II. SENSOR PRINCIPLE

SMES adopts the same sensor as DMES. Figure 1(a) is the sensor's schematic diagram. The sensor can be divided into two parts: A silicon-based microstructure in which the beams and a mass block are interconnected, a rigid cilium glued on the mass block. The cilium mimics the stereocilia of fish's neuromast organ. The silicon-based microstructure mimics the hair cell of fish's neuromast [14]. The sensor's geometric parameters are marked on the cross-section of one side of it, as shown in Figure 1(b).

When the structure is deformed by pressure, the stress at a point on the centerline of the sensor's deformed beam can be expressed as [14]:

$$\sigma_{(x)} = \pm \left[\frac{L^2 + 3aL - 3x(a+L)}{\frac{2}{3}bt^2(L^2 + 3aL + 3a^2)} \pm \frac{1}{bt} \right] P \cdot S \quad (1)$$

where x represents the distance between the point and the frame, P represents pressure value reach to the cilium, S rep-

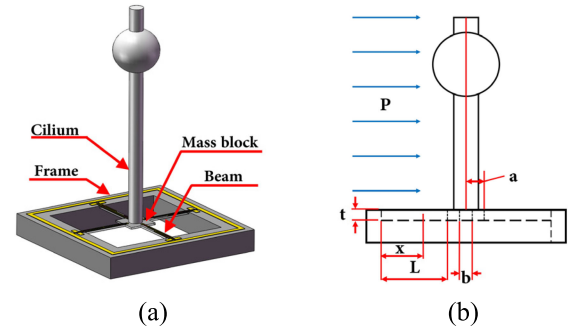


FIGURE 1. (a) The bionic sensor (b) Geometric parameter schematic of the sensor.

TABLE 1. Geometric parameters of sensor.

| | |
|---|--------------|
| Half-length of the center block's side(a) | 300 μ m |
| Width of beams(b) | 120 μ m |
| Thickness of beams(t) | 20 μ m |
| Length of beams(L) | 1000 μ m |

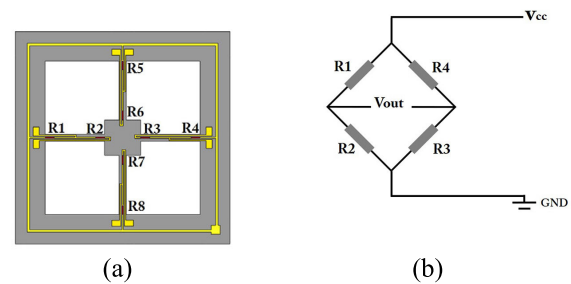


FIGURE 2. (a) Distribution of piezoresistors on four beams (b) The Wheatstone bridge composed of piezoresistors on the set of symmetrical beams used by stethoscope.

resents the surface area of cilium under pressure, respectively. The sensor's geometric parameters are shown in Table 1.

It can be derived from the formula that as S increases, the deformed beam's stress will also increase. Figure 1(a) shows that this sensor's cilium is a cylinder with a sphere compared with the original shaped sensor's cylinder cilium. The sphere increases S , which means the stress on the sensor beam is higher than the original sensor beam under the same pressure. Higher stress means greater resistance variation of piezoresistors distributed on the beam, eventually leading to a higher voltage output of the Wheatstone bridge composed of these piezoresistors. The sensitivity of this sensor is, therefore, improved. Figure 2(a) shows the piezoresistors arrangement on the silicone-based microstructure of the sensor.

The sensors are located in the center of the two packaging of DMES and SMES; figure 3(a) shows the sensor's location in DMES. After packaged with diaphragms and filled with silicone oil, DMES can measure heart sound, as shown in Figure 3(b). During auscultation with DMES, the bottom diaphragm should be close to the chest, and the added top diaphragm should be close to the air.

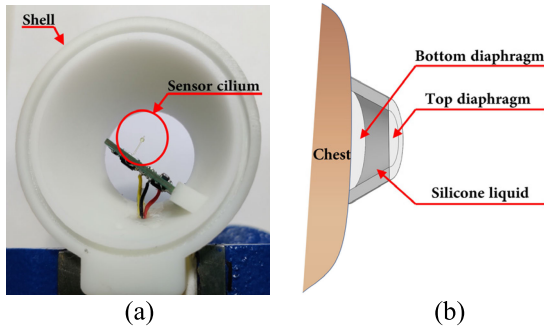


FIGURE 3. (a) Partially encapsulated DMES (b) DMES’s auscultation schematic diagram.

When heart sounds transfer into the packaging through the bottom diaphragm, the pressure is transmitted to the cilium, causing the cilium movement. Subsequently, the movement causes the deformation of the four-beam microstructure. The four beams are divided into two groups, two beams in each group are symmetrical along the mass block; Wheatstone bridges are distributed on each group and share a common power supply. To meet the auscultation requirements, DMES obtains scalar information: the amplitude of heart sound. Therefore, only a set of Wheatstone bridge is used as the sensor signal output; the Wheatstone bridge and the piezoresistors that make it up are shown in Figure 2(b). The symmetrical beams corresponding to these piezoresistors are placed in the same direction as the sound source, parallel to the bottom diaphragm. In this way, the acoustic sensor performs the maximum acoustoelectric conversion and achieves auscultation application.

III. PACKAGING DESIGN
A. PACKAGING PRINCIPLE

The interiors of single diaphragm packaging and double-sided diaphragm packaging are filled with silicone oil to form a kind of fluid-solid coupling encapsulation, which reduces the heart sound attenuation. Nitrile butadiene rubber (NBR), which has been proven to own excellent sound transmission performance and broad frequency band, is adopted as the diaphragm material of single and double-side diaphragm packaging [15]–[17]. The introduction of the top diaphragm of double-sided diaphragm packaging makes it have different acoustic performance than the single diaphragm packaging. Figure 4 shows the transmission path of the heart sound in the packagings; the incident interface is the contact interface between packagings and the human body, representing the bottom diaphragm of DMES and the only diaphragm of SMES. The reflection interface represents the top diaphragm of DMES and the shell bottom of SMES; the sound will be reflected when it reaches. The sound reflectivity depends on the acoustic impedance ratio between two media on both sides of the reflection interface [15]. For DMES, the media on both sides of the reflection interface are silicone oil and air, and due to the diaphragm’s silicone oil impermeability and sound transmission ability, which form a water-air interface. The

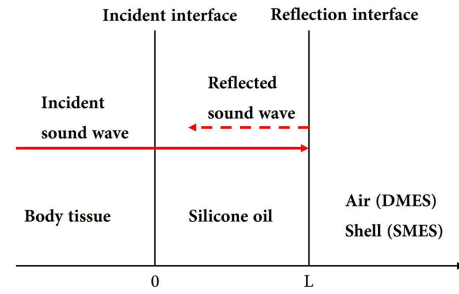


FIGURE 4. The schematic diagram of the transmission of the heart sound.

water-air interface is called a “pressure release” or “soft” surface for the underwater sound as it is usually an almost perfect reflector of acoustic waves [18], [19]. For SMES, these two media are silicone oil and shell material. The acoustic impedance ratio between the two media is three orders of magnitude smaller than that between silicone oil and air. It also means that the reflectivity of sound at the shell bottom of SMES is much lower than that at the top diaphragm of DMES. Because the impedance of body tissue, the diaphragm, and silicone oil are close, heart sounds pass through the incident interface almost without loss; when it reaches the reflection interface, the reflected wave interferes with it.

For DMES, the interference significantly increases sound pressure inside the shell, which means that the sensor has to bear more significant sound pressure. Heart sound signal can be considered to be composed of countless pulse signals with different frequencies. Providing a pulse signal $\delta(t)$ of heart sound signal returns and interferes with the original pulse signal after Δt seconds, then it can be $g(t) = \delta(t) + q\delta(t - \Delta t)$. Wherein q is the reflection coefficient. Set $q = 1$, by Fourier transform, the power spectrum is obtained as follows:

$$|G(f)| = 2 |\cos(\omega\Delta t)/2| \tag{2}$$

Figure 5 shows the graph of the power spectrum in log ordinate. Zero-point must satisfy $f = (n + 1)/2\Delta t, n = 0, 1, 2 \dots$. Providing that $\Delta t = 0.05\text{ms}$, then $f = 10000\text{Hz}$. As the depth of the packaging shell of DMES is 2cm, which is very shallow, the return time Δt is far less than 0.05ms, which means that in the frequency range of 20-6000Hz, the original sound pressure level inside the shell will be amplified, with a maximum increase of 6dB.

B. FINITE SIMULATION

The double-sided diaphragm packaging’s superiority is verified by comparing it with the single diaphragm packaging. When single diaphragm packaging and double-sided diaphragm packaging are in the same sound field, the pressures inside them are different, and the pressure difference is our concern. Silicone oil is the encapsulated liquid inside the packagings, in which only the longitudinal wave exists. In terms of the transverse wave in the diaphragms,

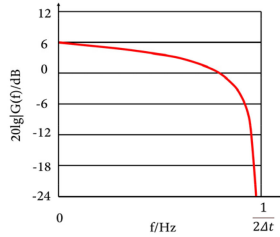


FIGURE 5. The spectrum of the interference between reflected wave and original wave.

TABLE 2. Materials' properties used in the simulation.

| | Silicone oil | Air | NBR (diaphragm) | C-VU (shell) |
|-----------------------------|--------------|-------|--------------------|-----------------|
| Density(kg/m ³) | 963 | 1.293 | 1065 | 1120 |
| Velocity(m/s) | 1450 | 343 | N/A | N/A |
| Poisson coefficient | N/A | N/A | 0.47 | 0.45 |
| Elastic modulus(MPa) | N/A | N/A | 2460 | 2050 |

since the sound source is perpendicular to the structure, the transverse wave generated in the diaphragms is so small that it can be ignored. The acoustic wave equation describing the pressure distribution in liquid in the frequency domain can be written as:

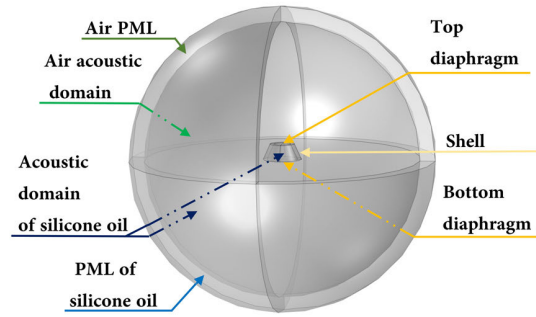
$$\nabla \cdot \left(-\frac{1}{\rho_0} (\nabla p - q) \right) - \frac{\omega^2 p}{\rho_0 c^2} = Q \quad (3)$$

where ρ_0 is the density of the fluid, c is the velocity of sound in liquid, ω is the angular frequency, p is sound pressure, q and Q represent dipole source and monopole source, respectively. When there's neither monopole nor dipole source. The equation can be expressed as:

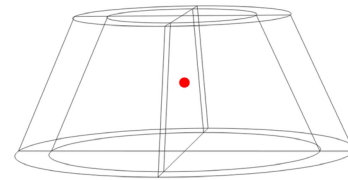
$$\nabla \cdot \left(-\frac{1}{\rho_0} \nabla p \right) - \frac{\omega^2 p}{\rho_0 c^2} = 0 \quad (4)$$

Based on the equation above, the finite element models of the sound field of double-sided diaphragm packaging and single diaphragm packaging are established simultaneously in COMSOL Multiphysics (Stockholm, Sweden). The process of modeling will be briefly discussed.

Figure 6(a) shows the sound field simulation geometric model of DMES. The packaging is simplified and only contains the main parts. The model's sound field is set as a sphere, the upper hemisphere simulates air, and the lower hemisphere simulates the semi-infinite medium human body. Two perfectly matched layers are used to match these two hemispheres to eliminate the effect of boundary, creating the ideal situation without unnecessary acoustic reflection. Because silicone oil's acoustic characteristics are similar to that of the human body, the human body is replaced by silicone oil in this model [16], [23], [24]. The properties of materials are shown in Table 2.



(a)



(b)

FIGURE 6. (a) Simulation geometric model of DMES (b)The pressure value extraction point.

The acoustic domain is divided into two parts by DMES packaging, the internal and external. The boundary condition is set as a plane wave of 1 pa propagating vertically to the bottom diaphragm from the silicone oil acoustic domain. The variation curve of sound pressure with frequency inside packaging is the focus of attention. A point is set in the internal acoustic domain center in the post-processing of simulation results, where the sensor's cilium is located. The point is marked in red in Figure 6(b). Then the sound pressure level (SPL) of this point is extracted. As for SMES, its sound field modeling and the post-processing of simulation follow the same steps as DMES. The variation curves of SPL versus frequency at extraction points of these two models are shown in Figure 7. Besides, Figure 8 shows the sound pressure level distribution in the cross-sections of the DMES and SMES. It can be seen that in the main frequency band of heart sound, the SPL of DMES is about 4 dB higher than that of SMES.

IV. FABRICATION AND TESTING

A. FABRICATION

The sensor is divided into two parts: the lollipop-shaped cilium and the cross-beam structure. The lollipop-shaped cilium is made by high-precision 3D printing technology, using high-temperature resistant resin as printing material. The cross-beam structure is fabricated by MEMS technology, using a 4-inch N-type SOI silicon wafer. The thickness of the embedded oxygen layer is 2um, the thickness of the top silicon layer is 20um, and the thickness of the substrate layer is 400um. The brief fabrication process of the cross-beam

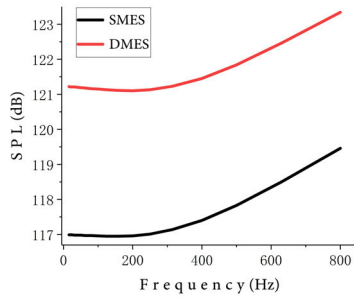


FIGURE 7. The variation curves of SPL with frequency at extraction points of SMES and DMES.

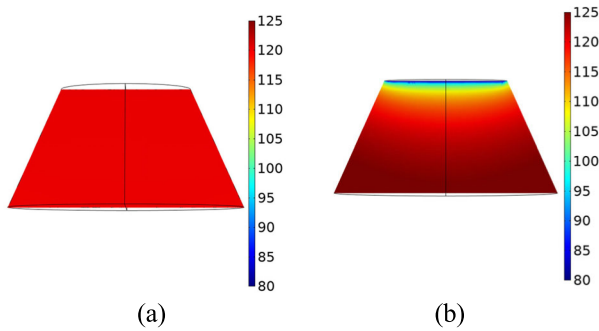


FIGURE 8. The SPL cross-section of (a) SMES (b) DMES.

structure is shown in Figure 9. (a) SOI wafer is oxidized at 950°C to form 200nm silicon dioxide layer; (b) The resistance bar windows are obtained by ICP (Inductively Coupled Plasma) etching silicon dioxide and then (c) implants boron (100Kev, $4 \times 10^{18} \text{cm}^{-3}$) to form the piezoresistors; (d) Re-oxidization, ICP etching silicon dioxide and implanting heavy boron ($100\text{Kev}, 4 \times 10^{21} \text{cm}^{-3}$) to form the P + area; (e) Depositing silicon nitride (150nm) via PECVD (Enhanced Chemical Vapor Deposition), ICP etching silicon nitride and depositing Au(100 nm), then etching Au via iodine solution to form the Wheatstone Bridge; (f) Frontal etching and back etching to release the structure [20]. Then on the micro-system integration platform, the cilium and the cross-beam structure are integrated with UV glue to form the whole sensor, as shown in Figure 10. Subsequently, the entire sensor is fixed on the PCB with the pre-processing circuit. The PCB board is set in the appropriate position of the packaging shell, as mentioned before.

The sound intensity of heart sound is very low, less than 15 dB, so the sensor’s output is amplified and filtered by the PCB board’s pre-processing circuit. The sensor’s output is amplified 497 times by using the instrument amplifier chip AD8226. Since the frequency band of heart sound signal is mainly concentrated in 20-600hz, the signal beyond 14-1000hz is filtered by the filter chip AD823A. The final processed signal can then be transmitted to the upper computer for display through data acquisition and transmission

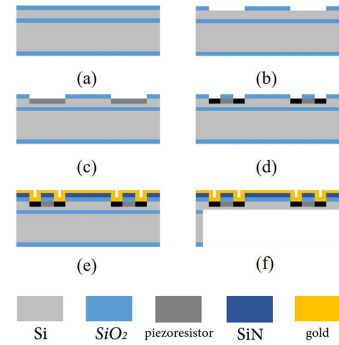


FIGURE 9. Schematic diagram of the four-beam microstructure manufacturing process.

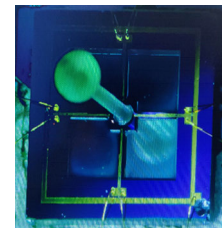


FIGURE 10. The whole sensor.

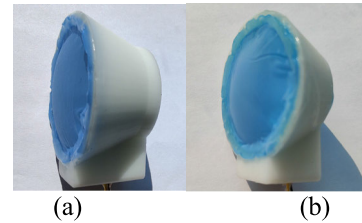


FIGURE 11. (a) A SMES (b) A DMES.

equipment. Both SMES and DMES were fabricated, as shown in Figure 11.

B. FEASIBILITY TEST

The systolic and diastolic cycles produce vibration with different frequencies. The visualizing of these vibrations is the phonocardiogram. Figure 12 shows the phonocardiogram of DMES displayed by the upper computer; this heart sound segment was collected from a normal person’s tricuspid valve area. The auscultation area was determined by a doctor, and the subject was Mr. Duan, 24, who is supine during the test. The subject was measured by both DMES and 3M. The diastolic and systolic periods are marked in the figure. S_1, S_2 represent first heart sound and second heart sound, respectively, S_{12} represents the time interval between S_1 and S_2 , S_{21} is the opposite. It can be seen that the amplitude of S_1 is higher than S_2 , and the ratio of the time interval (S_{12} and S_{21}) is about 0.5, the diastole is longer than the systolic simultaneously. All these show that the normal heart sound measured by DMES is consistent with the theory [21].

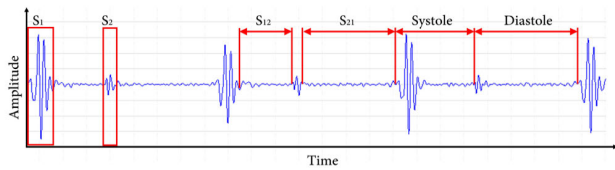


FIGURE 12. Heart sound signal of normal people.

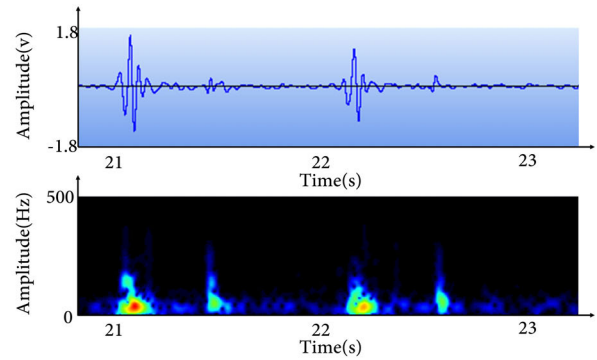


FIGURE 15. One section of heart sound measured by 3M and its spectrogram.

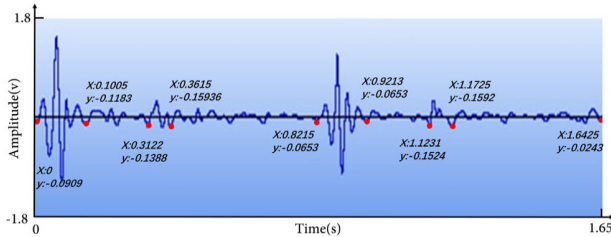


FIGURE 13. The time-domain waveform of the 3M electronic stethoscope.

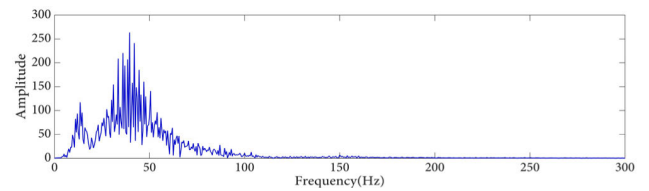


FIGURE 16. The spectrum diaphragm of DMES.

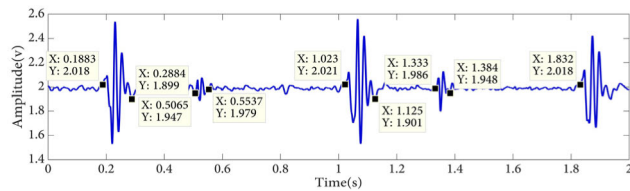


FIGURE 14. The time-domain waveform of DMES.

TABLE 3. Two kinds of heart sound signals' Time-domain statics.

| | S ₁ (s) | S ₂ (s) | S ₁₂ (s) | S ₂₁ (s) | Sys- tole(s) | Dias- tole (s) | S _T (s) |
|------|--------------------|--------------------|---------------------|---------------------|-----------------|-------------------|--------------------|
| 3M | 0.101 | 0.049 | 0.212 | 0.460 | 0.312 | 0.509 | 0.822 |
| 3M | 0.998 | 0.049 | 0.202 | 0.470 | 0.302 | 0.520 | 0.825 |
| DMES | 0.100 | 0.047 | 0.218 | 0.448 | 0.318 | 0.499 | 0.817 |
| DMES | 0.102 | 0.051 | 0.208 | 0.469 | 0.310 | 0.517 | 0.827 |

Subsequently, the heart sound signal collected by DMES was compared with that of 3M electronic stethoscope in the time and frequency domain. 3M has its software that can display the waveform of heart sound and save data; however, it cannot precisely show the time-domain information. Therefore, the time domain waveform of 3M was imported into Origin (Northampton, USA) to get accurate time information using its digitizing function. Figure 13 shows the visualization image of the heart sound signal collected by 3M. Red spots are used to mark each heart sound's beginning and end, and its coordinate information is attached around.

The original data collected by DMES was imported into MATLAB to draw the heart sound waveform and carried out time-domain annotation, as shown in Figure 14. Table 3 shows the time domain statistics of two kinds of heart sound signals.

It is easy to see that heart sound signals measured by DMES is highly consistent with that of the 3M electronic

stethoscope in the time domain; therefore, the signal measured by DMES is reliable in the time domain.

The software of 3M can display the spectrogram of heart sound; the spectrogram is a visual representation of the spectrum of frequencies of heart sound signal as it varies with time. One section of the heart sound waveform of 3M and its corresponding spectrogram is shown in Figure 15.

According to the corresponding relationship on the time axis, the heart sound signal's energy is mainly concentrated in the period of first and second heart sounds. It also can be roughly seen that there is an energy concentration below 100 Hz and a little component between 100 and 250Hz. The heart sound signal measured by DMES was also analyzed using the Fourier transform; its spectrum diagram is shown in Figure 16. The figure shows that the energy is concentrated just below 100Hz, and there is almost no component after 100Hz, which is consistent with the 3M spectrogram. Therefore, the heart sound signal measured by DMES is reliable in both the time domain and the frequency domain, which proves its feasibility.

C. SNR CONTRAST

The intelligent diagnosis of heart disease is based on the analysis of heart sound signals; however, if the SNR of the collected heart sound signal is not high enough, the useful information may be covered by the noise, thus affecting the disease's diagnosis. Therefore, SNR is an important index to measure the electronic stethoscope and can be expressed as:

$$SNR = 20\lg\left(\frac{\overline{u_s}}{\overline{u_n}}\right) \quad (5)$$

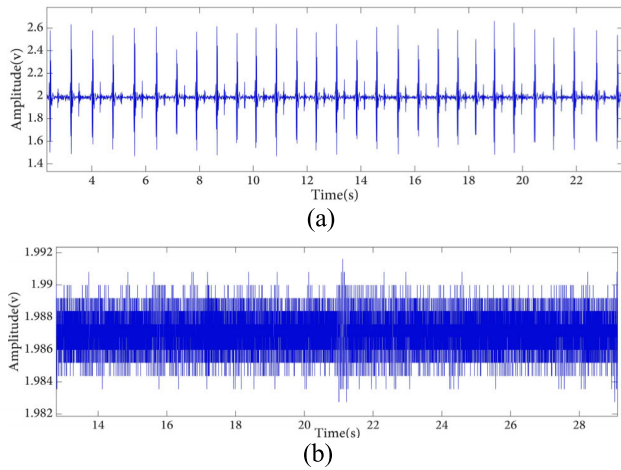


FIGURE 17. Heart sound signals of normal people detected by DMES: (a) Heart sound waveform diagram; (b) Noise signal without heart sound.

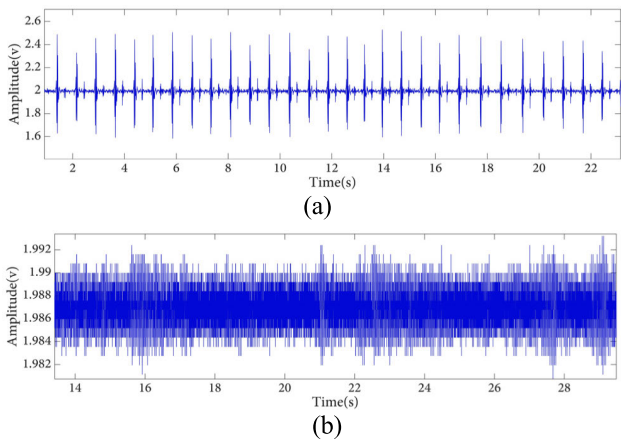


FIGURE 18. Heart sound signals of normal people detected by SMES: (a) Heart sound waveform diagram; (b) Noise signal without heart sound.

TABLE 4. The SNR related values of these three stethoscopes.

| | $\overline{u_s}(V)$ | $\overline{u_n}(V)$ | SNR (dB) |
|------|---------------------|---------------------|----------|
| 3M | 2.25±0.02 | 0.063±0.005 | 31.1 |
| DMES | 1.05±0.04 | 0.009±0.001 | 41.3 |
| SMES | 0.81±0.05 | 0.009±0.001 | 39.1 |

$\overline{u_s} = \sum_{s=1}^N u_s/N$, u_s is the peak value of the collected heart sound signal, u_n is the peak value of the collected noise signal, the noise signal is the static noise of the stethoscope without a heart sound signal. SMES, DMES, and 3M electronic stethoscope were used to collect heart sound signals and noise signals for 15 cycles, that is $N = 15$. The heart sound waveforms are shown in Figures 17, 18, and 19. Table 4 shows the results calculated by the formula.

V. DISCUSSION

When comparing stethoscopes' performance, the sensitivity between them is not compared. However, the sensitivity value is a more accurate parameter to measure the stethoscope's performance. The stethoscope sensitivity unit is the

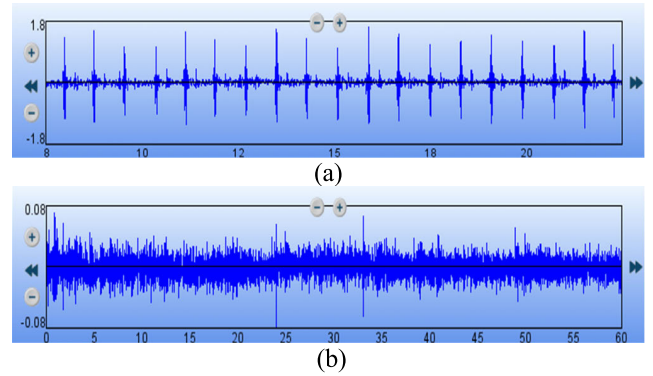


FIGURE 19. Heart sound signals of normal people detected by 3M electronic stethoscope: (a) Heart sound waveform diagram; (b) Noise signal without heart sound.

output voltage per mechanical input, i.e., V/mm. Toda and Thompson [22] proposed a measurement method in which the stethoscope is placed on a vibrating table. The stethoscope's sensitivity is obtained by dividing the stethoscope's voltage output by the displacement of the vibration table measured by an accelerometer. There is still no standard stethoscope sensitivity test method. Thus, the sensitivity test was not conducted in this paper. Besides, the packaging shell material used in the research is only for experiments, and the engineering materials are steel and aluminum alloy, which can further improve the SNR of the stethoscope

VI. CONCLUSION

This paper successfully uses a bionic sound-sensitive unit to design an electronic stethoscope and uses a double-sided diaphragm packaging as the stethoscope's packaging. Finite element simulation results show that double-sided diaphragm packaging's internal sound pressure level is about 4db higher than that of single diaphragm packaging. And SNR comparison shows that DMES's SNR is 2.2dB higher than SMES and 10.2 dB higher than the 3M electronic stethoscope. The DMES's feasibility was also verified by analyzing the collected heart sound signals in the time and frequency domain.

REFERENCES

- [1] A. Alwan, *Global Status Report on Noncommunicable Diseases 2010*. Geneva, Switzerland: World Health Organization, 2011.
- [2] P. S. Molcer, I. Kecskes, V. Delic, E. Domijan, and M. Domijan, "Examination of formant frequencies for further classification of heart murmurs," in *Proc. IEEE 8th Int. Symp. Intell. Syst. Informat.*, Sep. 2010, pp. 575–578.
- [3] P. Sharma, S. A. Imtiaz, and E. Rodriguez-Villegas, "Acoustic sensing as a novel wearable approach for cardiac monitoring at the wrist," *Sci. Rep.*, vol. 9, no. 1, pp. 1–13, Dec. 2019.
- [4] S. Leng, R. S. Tan, K. T. C. Chai, C. Wang, D. Ghista, and L. Zhong, "The electronic stethoscope," *Biomed. Eng. Online*, vol. 14, no. 1, pp. 1–37, 2015.
- [5] M. Zuber, "Acoustic cardiography to improve detection of coronary artery disease with stress testing," *World J. Cardiol.*, vol. 2, no. 5, p. 118, 2010.
- [6] M. Akay, A. Dragomir, Y. M. Akay, F. Chen, A. Post, H. Jneid, D. Paniagua, A. Denktas, and B. Bozkurt, "The assessment of stent effectiveness using a wearable beamforming MEMS microphone array system," *IEEE J. Transl. Eng. Health Med.*, vol. 4, pp. 1–10, 2016.
- [7] C. Smith, "Transducer for sensing body sounds," U.S. Patent 7 940 937, May 10, 2011.

- [8] B. Grundlehner and D. Buxi, "Methods to characterize sensors for capturing body sounds," in *Proc. Int. Conf. Body Sensor Netw.*, May 2011, pp. 59–64.
- [9] R. Baptista, H. Silva, and M. Rocha, "Design and development of a digital stethoscope encapsulation for simultaneous acquisition of phonocardiography and electrocardiography signals: The smarthear case study," *J. Med. Eng. Technol.*, vol. 44, no. 4, pp. 1–9, 2020.
- [10] M. Zhang, G. Wu, D. Ren, R. Gao, Z.-M. Qi, and X. Liang, "An optical MEMS acoustic sensor based on grating interferometer," *Sensors*, vol. 19, no. 7, p. 1503, Mar. 2019.
- [11] W. R. Ali and M. Prasad, "Design and fabrication of microtunnel and Si-diaphragm for ZnO based MEMS acoustic sensor for high SPL and low frequency application," *Microsyst. Technol.*, vol. 21, no. 6, pp. 1249–1255, Jun. 2015.
- [12] S. C. Ko, C.-H. Jun, W. I. Jang, and C.-A. Choi, "Micromachined air-gap structure MEMS acoustic sensor using reproducible high-speed lateral etching and CMP process," *J. Micromech. Microeng.*, vol. 16, no. 10, p. 2071, 2006.
- [13] C. Xue, S. Chen, W. Zhang, B. Zhang, G. Zhang, and H. Qiao, "Design, fabrication, and preliminary characterization of a novel MEMS bionic vector hydrophone," *Microelectron. J.*, vol. 38, nos. 10–11, pp. 1021–1026, Oct. 2007.
- [14] Y. Liu, R. Wang, G. Zhang, J. Du, L. Zhao, C. Xue, W. Zhang, and J. Liu, "'Lollipop-shaped' high-sensitivity microelectromechanical systems vector hydrophone based on parylene encapsulation," *J. Appl. Phys.*, vol. 118, no. 4, Jul. 2015, Art. no. 044501.
- [15] M. Liu, Z. M. Jian, G. Zhang, N. Guo, and W. Zhang, "Design of MEMS bionic vector hydrophone based on NBR sound-transparent cap," *Sensor Rev.*, vol. 35, no. 3, pp. 303–309, Jun. 2015.
- [16] G. Zhang, Q. Xu, C. Zhang, S. Chen, and S. Yang, "Optimization of shell packaging for cilium MEMS bionic vector hydrophone," *Sens. Actuators A, Phys.*, vol. 306, May 2020, Art. no. 111969.
- [17] Z. Guojun, W. Panpan, G. Linggang, X. Jijun, and Z. Wendong, "Improvement of the MEMS bionic vector hydrophone," *Microelectron. J.*, vol. 42, no. 5, pp. 815–819, May 2011.
- [18] O. A. Godin, "Sound transmission through water–air interfaces: New insights into an old problem," *Contemp. Phys.*, vol. 49, no. 2, pp. 105–123, Mar. 2008.
- [19] A. Bolghasi, P. Ghadimi, and M. A. F. Chekab, "Low-frequency sound transmission through rough bubbly air–water interface at the sea surface," *J. Low Freq. Noise, Vib. Act. Control*, vol. 36, no. 4, pp. 319–338, Dec. 2017.
- [20] L. Zhang, Q. Xu, G. Zhang, R. Wang, Y. Pei, W. Wang, Y. Lian, S. Ji, and W. Zhang, "Design and fabrication of a multipurpose cilia cluster MEMS vector hydrophone," *Sens. Actuators A, Phys.*, vol. 296, pp. 331–339, Sep. 2019.
- [21] M. V. Shervegar and G. V. Bhat, "Automatic segmentation of phonocardiogram using the occurrence of the cardiac events," *Informat. Med. Unlocked*, vol. 9, pp. 6–10, Jan. 2017.
- [22] M. Toda and M. L. Thompson, "Contact-type vibration sensors using curved clamped PVDF film," *IEEE Sensors J.*, vol. 6, no. 5, pp. 1170–1177, Oct. 2006.
- [23] B. Altun, I. Demirkan, E. O. Isik, O. Kocaturk, M. B. Unlu, and B. Garipcan, "Acoustic impedance measurement of tissue mimicking materials by using scanning acoustic microscopy," *Ultrasonics*, vol. 110, Feb. 2021, Art. no. 106274.
- [24] F. Sabri, M. E. Sebelik, R. Meacham, J. D. Boughter, M. J. Challis, and N. Leventis, "In vivo ultrasonic detection of polyurea crosslinked silica aerogel implants," *PLoS ONE*, vol. 8, no. 6, Jun. 2013, Art. no. e66348.



WEIDONG WANG received the B.S. degree from the School of Measurement and Control Technology and Instrument, Shengyang Institute of Engineering, in 2017. He is currently pursuing the master's degree with the Laboratory of Science and Technology on Electronic Test and Measurement, North University of China, with a focus on MEMS devices applied in acoustic transducers.



SAI ZHANG received the B.S. degree in electronic information science and technology from the North University of China, Taiyuan, China, in 2004, and the Ph.D. degree in marine science (marine physics) from Xiamen University, Xiamen, China, in 2006. From 2016 to 2019, he was a Lecturer with the Department of Physics, Jiangsu University, Zhenjiang, China. Since 2019, he has been an Associate Professor in physics with Jiangsu University. He is currently holds a postdoctoral position in instrument science and technology with the North University of China. His research interests include sonic crystals, acoustic metamaterials, acoustic sensors, and so on.



XI YANG received the B.S. degree from the North University of China, China, in 2018. She is currently pursuing the master's degree with the State Key Laboratory of Dynamic Testing Technology, North University of China, with a focus on MEMS devices applied in acoustic transducers.



YU ZHANG received the B.S. degree from the North University of China, Taiyuan, China, in 2012, where she is currently pursuing the M.E. degree in instrument science and technology. Her research interest includes ultrasound computer tomography.



GUOJUN ZHANG received the B.S. degree from the Department of Automatic Control, North China Institute of Science and Technology, in July 2001, and in microelectronics from the Department of Microelectronics, Tsinghua University, in September 2001, the M.S. degree from the Institute of Acoustics, Chinese Academy of Sciences, with a focus on nonlinear acoustics of perforated panel structure, and the Ph.D. degree from Northwestern Polytechnical University, in 2015. Since 2016, he has been a Postdoctoral Fellow with Harbin Engineering University. His main research interest includes MEMS vector hydrophone.



SICUN DUAN received the B.S. degree from the School of Electrical and Control Engineering, Heilongjiang University of Science and Technology, in 2018. He is currently pursuing the master's degree in instrument science and technology with the North University of China, Shanxi, China. His main research interest includes MEMS devices applied in acoustic transducers.